Polymers **2015**, *7*, 1497-1509; doi:10.3390/polym7081466

OPEN ACCESS

polymers

ISSN 2073-4360

www.mdpi.com/journal/polymers

Article

Roughening Conjugated Polymer Surface for Enhancing the Charge Collection Efficiency of Sequentially Deposited Polymer/Fullerene Photovoltaics

Yoonhee Jang [1], Ji-Won Seo [2], Jeesoo Seok [1], Jung-Yong Lee [2] and Kyungkon Kim [1,*]

[1] Department of Chemistry and Nano Science, Ewha Womans University, Seoul 127-750, Korea; E-Mails: unee38@ewhain.net (Y.J.); zsoo@ewhain.net (J.S.)

[2] Graduate School of Energy, Environment, Water, and Sustainability (EEWS), Graphene Research Center, Korea Advanced Institute of Science and Technology (KAIST), Daejeon 305-701, Korea; E-Mails: jiwonseo@kaist.ac.kr (J.-W.S.); jungyong.lee@kaist.ac.kr (J.-Y.L.)

* Author to whom correspondence should be addressed; E-Mail: kimkk@ewha.ac.kr; Tel.: +82-2-3277-3429; Fax: +82-2-3277-2384.

Academic Editors: Christian B. Nielsen and Laure Biniek

Received: 25 May 2015 / Accepted: 6 August 2015 / Published: 13 August 2015

Abstract: A method that enables the formation of a rough nano-scale surface for conjugated polymers is developed through the utilization of a polymer chain ordering agent (OA). 1-Chloronaphthalene (1-CN) is used as the OA for the poly(3-hexylthiophene-2,5-diyl) (P3HT) layer. The addition of 1-CN to the P3HT solution improves the chain ordering of the P3HT during the film formation process and increases the surface roughness of the P3HT film compared to the film prepared without 1-CN. The roughened surface of the P3HT film is utilized to construct a P3HT/fullerene bilayer organic photovoltaic (OPV) by sequential solution deposition (SqSD) without thermal annealing process. The power conversion efficiency (PCE) of the SqSD-processed OPV utilizing roughened P3HT layer is 25% higher than that utilizing a plain P3HT layer. It is revealed that the roughened surface of the P3HT increases the heterojunction area at the P3HT/fullerene interface and this resulted in improved internal charge collection efficiency, as well as light absorption efficiency. This method proposes a novel way to improve the PCE of the SqSD-processed OPV, which can be applied for OPV utilizing low band gap polymers. In addition, this method allows for the reassessment of polymers, which have shown insufficient performance in the BSD process.

Keywords: organic photovoltaics; bilayer organic photovoltaics; sequential deposition; ordering agent

1. Introduction

The bulk heterojunction (BHJ) is the most-used active layer system in organic photovoltaic (OPV) devices. Usually, the blended solution, in which both the electron donating polymer and the electron accepting fullerene derivatives homogeneously mixed, is used to form the BHJ. The blended solution deposition (BSD) process is effective in the formation of the BHJ with a large surface area in a single layer [1]. However, delicate control of the processing conditions (including the donor–acceptor ratio, the amount of processing additives, types of solvents, and processing temperature) are required to induce donor–acceptor phase separation at the nano-scale to maximize solar cell performance [2,3].

A sequential solution deposition (SqSD) of the electron donating polymer layer and the electron accepting fullerene layer can be utilized to form a polymer/fullerene heterojunction in OPV [4,5]. The SqSD process is more straightforward in facilitating device optimization compared to the BSD process. However, there are a few problems associated with the SqSD-processed polymer/fullerene layer.

The small heterojunction area at the polymer/fullerene interface and the limited availability of solvents for the top-layer solution that do not dissolve the bottom-layer are both problems that need to be addressed.

Poly(3-hexylthiophene)s (P3HT) are an important class of π-conjugated polymers that can be used in plastic electronic devices, such as solar cells and field-effect transistors. The P3HT can be ordered in three dimensions: conformational ordering along the backbone, π-stacking of flat polymer chains, and lamellar stacking between chains. All of these features lead to the excellent electrical properties of these materials [6,7]. Recently, many interesting reports on SqSD-processed polymer/fullerene OPVs based on P3HT and fullerene derivatives have been reported [4,5,8–15]. However, similar to a BSD-processed P3HT/fullerene OPVs, SqSD-processed P3HT/fullerene OPVs require a thermal annealing step to obtain a satisfactory heterojunction area. It would be desirable if the nano-structured polymer surface could first form a large area heterojunction with fullerene without the need for a thermal annealing step in the production of SqSD-processed P3HT/fullerene OPVs. Developing the polymer nanostructure using a poly(dimethylsiloxane) (PDMS) stamp is one possible method [16], but this method has its drawbacks. A simpler and cost effective method needs to be established that enables the formation of nano-scale polymer surfaces.

In this study, we have developed a way to increase the surface area of the P3HT film by roughening the surface of the polymer at the nano-scale through the utilization of a polymer chain ordering agent (OA). This roughened surface of the P3HT film was utilized to construct a P3HT/fullerene OPV by the SqSD process without the need for a thermal annealing step. This SqSD-processed P3HT/fullerene OPV with OA showed superior solar cell performance, compared to the SqSD-processed P3HT/fullerene OPV prepared without an OA. This method proposes a novel way to improve the PCE of the SqSD-processed OPV, which can be applied for OPV utilizing low band gap polymers.

2. Experimental Section

2.1. Device Fabrication

Pre-patterned indium tin oxide (ITO)-coated glass substrates (40 Ω/square) were cleaned by ultrasonic treatment for 10 min first in isopropyl alcohol (IPA), and then acetone, and the substrates were subsequently dried at 100 °C in a convection oven for 30 min. The cleaned substrates were treated by UV ozone for 20 min. The PEDOT:PSS (CleviosTM P VP AI 4083, Leverkusen, Germany) layer was spin-coated onto the cleaned substrate at a speed of 4000 rpm for 35 s, and the substrate was then dried at 100 °C in a vacuum oven for 10 min. The Poly(3-hexylthiophene) (P3HT) with regioregularity of 91%–94% (Rieke Metals Inc., Lincoln, NE, USA) was used as received. The P3HT solutions were prepared from a co-solvent of chlorobenzene (CB) (Aldrich, St. Louis, MO, USA) and 1-chloronaphthalene (1-CN) (Aldrich, St. Louis, Missouri, USA). The volume percent of 1-CN in the co-solvent was 0%, 2%, 4%, 6%, 10%, and 50%. The P3HT was dissolved in the corresponding co-solvent with the concentration of 14 mg/1 mL. The P3HT solution was spin-coated onto the PEDOT:PSS layer with a speed of 1000 rpm for 15 s, followed by drying at 110 °C in a vacuum oven for 60 min. A phenyl-C61-butyric-acid-methyl ester ($PC_{61}BM$) (Nano-C, Westwood, MA, USA) solution (3.5 mg/mL) was prepared in dichloromethane (DCM). The $PC_{61}BM$ layer was spin-coated on top of the P3HT layer with a speed of 2000 rpm for 10 s. Lithium fluoride (LiF) and aluminum (Al) electrodes were deposited via thermal evaporation at a deposition rate of ~0.5 nm/s to 100 nm thickness. LiF and Al were thermally evaporated at $\sim 3 \times 10^{-6}$ Torr through a shadow mask, and the device area was 0.12 or 0.20 cm^2.

2.2. Measurement

The current density *vs.* voltage (*J-V*) curves of the devices were measured using a Keithley 2400 source meter (Keithley Instruments, Inc., Cleveland, OH, USA) under AM 1.5 G irradiation from a Xenon lamp-based solar simulator (K201 LAB50, McScience Inc., Suwon, GyeongGi, Korea). The external quantum efficiency (EQE) results were acquired using a spectral measurement system (K3100 IQX, McScience Inc., McScience Inc., Suwon, GyeongGi, Korea). This system applied monochromatic light from a xenon arc lamp at 300 W filtered by a monochromator (Newport, Irvine, CA, USA) and an optical chopper (MC 2000 Thorlabs, Newton, NJ, USA). The photo flux was superimposed to the dark during the EQE measurement. Device reflectance (R_{device} (λ)) as a function of wavelength λ was determined by the sum of I_{sub} and I_{act}, where I_{sub} is the light intensity reflected by the glass and I_{act} is the light intensity escaped from the device after the absorption by the glass, active layer, and Al electrode, and re-absorption by the active layer. For the measurement of R_{device}, the device was located in the integrating sphere. The device was tilted at approximately 8° through an integration sphere. The light reflected by the glass (I_{sub}) and escaped from the device (I_{act}) were scattered in the integration sphere and collected by a photodetector located in the integration sphere. The absorption by the device was extracted from the measured wavelength-dependent reflectance data. The internal quantum efficiency (IQE) as a function of wavelength λ was determined as follows: IQE (λ) = EQE (λ)/[1 − R_{device} (λ)]. UV-visible absorption spectra were obtained by UV-2450 (Shimadzu, Nakagyo-ku, Kyoto, Japan). Atomic force microscopy (AFM) images were obtained in tapping mode using an XE-70 atomic force microscope

(Park Systems Corp., Suwon, GyeongGi, Korea). To obtain the surface area of those films, the total surface areas of each film was obtained by using the software installed in the operation program of XE-70, and the surface area of each film was obtained after excluding the geometric area (5 μm × 5 μm) from the total surface area.

3. Results and Discussion

1-CN was used as an OA for the polymer bottom layer in the SqSD-processed bilayer OPV. 1-CN has been used as a processing additive in the blended solution of polymer and fullerene to fabricate BHJ OPVs [17–21]. According to Beaujuge *et al.* solution-processing methods involving low vapor pressure co-solvents are useful in terms of inducing the formation of favorable nano-scale morphologies [19]. Hoven *et al.* also reported that an additive with a high boiling point and low vapor pressure reduces the evaporation kinetics of the co-solvent and provides control over the morphology of the active layer [20].

Based on these previous reports on the incorporation of additives into the BHJ film, incorporation of the low vapor pressure 1-CN to the host solvent could afford the polymer chains more time to become ordered by reducing the evaporation rate of the host solvent. In addition, unlike with other additives, the planar π-conjugated structure of 1-CN could assist the ordering of the conjugated polymers, such as P3HT, during the film formation process.

To investigate the effect of 1-CN on the morphology of P3HT, the P3HT solutions were prepared from a co-solvent of chlorobenzene (CB) and 1-CN. The volume percent of 1-CN in the co-solvent was 0%, 2%, 4%, 6%, 10%, and 50%. Figure 1a,b displays the surface morphologies and height profiles of the P3HT films were prepared by utilizing the different solvent ratios scanned by atomic force microscope (AFM). The root mean square (RMS) roughness values of the P3HT films are summarized in Table 1, and Figure 1e displays the change in the RMS value of the P3HT films as a function of 1-CN concentration in the solvent. The roughness of the P3HT film increased as the concentration of 1-CN in the co-solvent increased to a maximum concentration of 4 vol % 1-CN. The roughness decreased as the concentration was increased beyond 4 vol % 1-CN. The maximum RMS of 4.7 nm was found from the P3HT film prepared by the co-solvent 96 vol % CB + 4 vol % 1-CN (Figure 1b), and the value is 52% larger than that of P3HT prepared with only CB (2.2 nm) (Figure 1a). Hereafter, the P3HT film prepared with the co-solvent 96 vol % CB and 4 vol % 1-CN will be denoted as P3HT(CB-CN), and that prepared with 100 vol % CB will be denoted as P3HT(CB).

The UV-VIS absorption spectra of as-prepared P3HT(CB) (square of Figure 2a) and P3HT(CB-CN) (circle of Figure 2a) are shown in Figure 2a. Both films show vibronic features in the wavelength range of 500–650 nm, which correspond to the ordered structures of P3HT [21]. The vibronic peak of the P3HT(CB-CN) was more intense than that of P3HT(CB). This suggests that P3HT(CB-CN) has more ordered P3HT domains than P3HT(CB). The X-ray diffraction (XRD) measurements on P3HT(CB) and P3HT(CB-CN) also support the UV-VIS absorption results. Figure 2b shows the XRD profile of the P3HT(CB) and P3HT(CB-CN) films. A distinct peak at a 2θ value of 5.3° was observed from the XRD profiles of both films. The peak at the 2θ value of 5.3° is related to the ordering of P3HT chains along the (110) direction and corresponds to the spacing between the P3HT lamellae [22,23]. The full width at half maximum (FWHM) of the peak from the P3HT(CB-CN) film (0.44 Å) is narrower than that from the P3HT(CB) (0.49 Å), which implies that the domain size of the ordered P3HT in the P3HT(CB-CN) is

larger than that of the P3HT(CB). Consequently, the addition of 1-CN increases the ordered domain size of the P3HT and results in the increased roughness and larger surface area observed in the P3HT(CB-CN) film. The roughened surface of the P3HT(CB-CN) will form a heterojunction with the $PC_{61}BM$ top-layer with a large interfacial area, which will enhance the solar cell efficiency by increasing the exciton dissociation efficiency [17]. We compared the absorption intensity of P3HT films after spin coating the DCM, the solvent for the $PC_{60}BM$ top-layer, on the P3HT film to investigate whether DCM dissolves the P3HT bottom-layer. The maximum absorbance of P3HT(CB) was reduced from 0.645 to 0.601 at 511 nm (6.8% reduction) and that of P3HT(CB-CN) was reduced from 0.614 to 0.567 at 511 nm (7.6% reduction) after spin coating on the corresponding films. Based on these results, it is expected that the ordered domain of P3HT will not be removed easily by the $PC_{61}BM$ solvent and will maintain its roughness even after the construction of the P3HT/$PC_{61}BM$ bilayer by the sequential solution process.

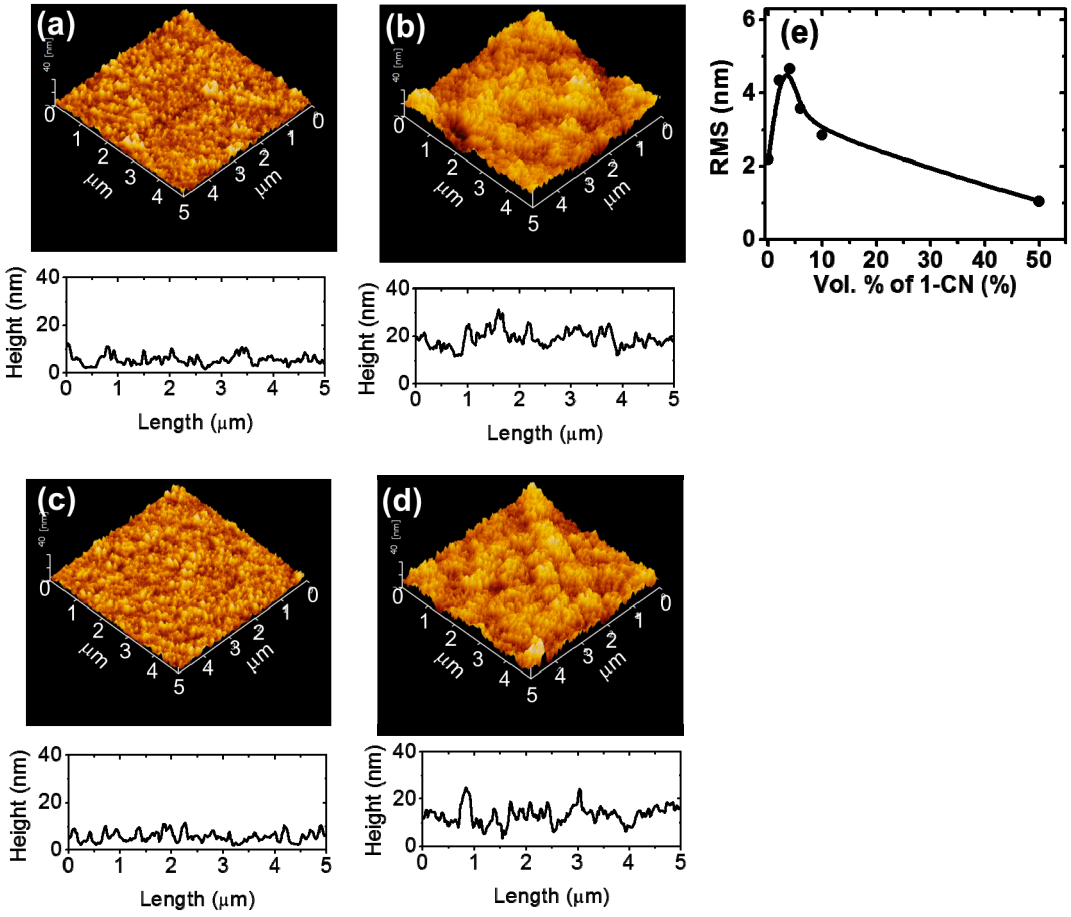

Figure 1. Surface morphologies and height profiles of the as prepared P3HT bottom-layer and the P3HT bottom-layer after removal of the PC61BM from the P3HT/PC61BM bilayer. (**a**) as prepared P3HT(CB); (**b**) P3HT(CB) bottom-layer after removal of the $PC_{61}BM$; (**c**) as prepared P3HT(CB-CN); and (**d**) P3HT(CB-CN) bottom-layer after removal of the $PC_{61}BM$; and (**e**) changes in the RMS of P3HT films as a function of the concentration of 1-CN in the CB solvent. All the AFM images were obtained via tapping mode with a scan dimension of 5 μm × 5 μm.

Table 1. RMS roughness and surface area data of P3HT films prepared from the CB solution containing different concentrations of 1-CN.

Film Description	vol % of 1-CN in CB	Increased Surface Area * ($\times$ 10^4 nm^2)	RMS (nm)
As prepared P3HT	0	7	2.2
	2	12	4.4
	4	13	4.7
	6	11	3.6
	10	12	2.9
	50	4	1.0
P3HT after removal of $PC_{61}BM$ from the P3HT/$PC_{61}BM$ film	0	9	2.1
	2	20	4.2

* The increased surface area of the films were calculated from the AFM images after excluding the geometric area (25 μm^2) from the total surface area.

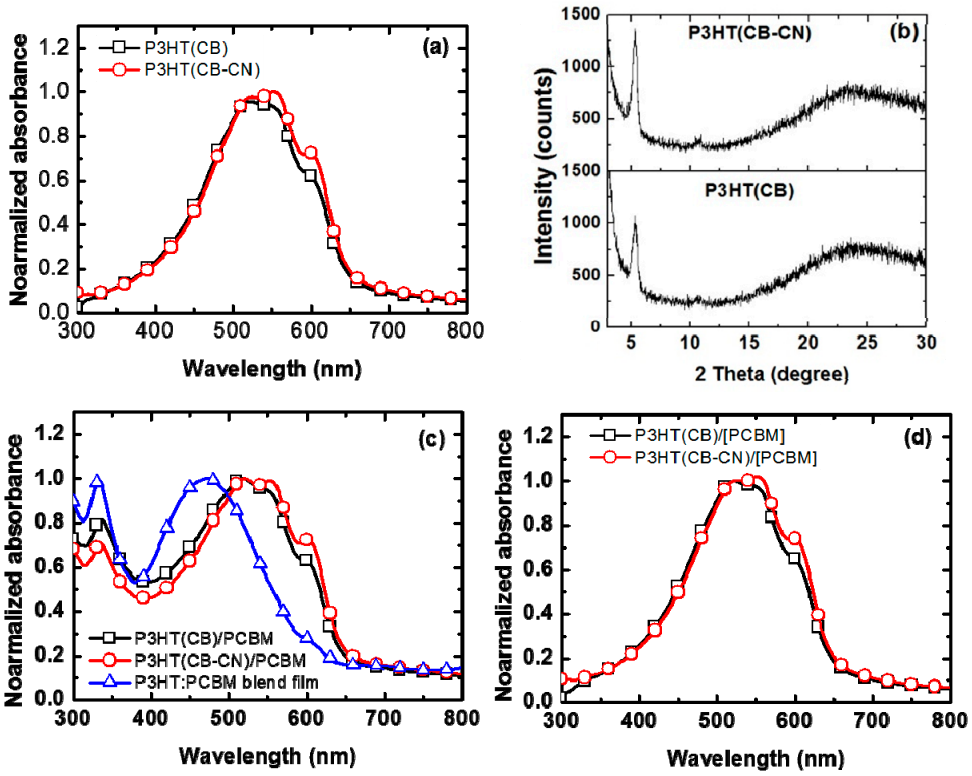

Figure 2. (**a**) UV-visible absorption spectra and (**b**) XRD profiles of P3HT(CB) and P3HT(CB-CN); (**c**) UV-visible absorption spectra of P3HT(CB)/$PC_{61}BM$ (square), P3HT(CB-CN)/$PC_{61}BM$ (circle) and P3HT:PCBM blend film; (**d**) UV-visible absorption spectra of P3HT(CB)/[$PC_{61}BM$] (square) and P3HT(CB-CN)/[$PC_{61}BM$] (circle).

The P3HT(CB)/$PC_{61}BM$ (square of Figure 2c) and P3HT(CB-CN)/$PC_{61}BM$ (circle of Figure 2c) bilayer films were prepared by the SqSD of the corresponding P3HT solution and $PC_{61}BM$ solution. UV-VIS absorption spectra of the bilayer films confirm that the $PC_{61}BM$ was successfully deposed on

the P3HT layer. Considering the reports on the SqSD-processed P3HT/PCBM film, the P3HT/PCBM is expected to form an inter-diffused bilayer instead of forming a bilayer with clear interface [5,11,12]. Interestingly, the P3HT/$PC_{61}BM$ bilayer film shows vibronic peaks from the P3HT at longer wavelengths, which is not observed in the P3HT:$PC_{61}BM$ BHJ film prepared from the blended solution of P3HT and $PC_{61}BM$ (triangle of Figure 2c). This implies that the ordering of the P3HT was not destroyed by the deposition of $PC_{61}BM$ layer, which is one of the important requirements in constructing a bilayer OPV. The absorption spectra of P3HT bottom-layer were obtained after selective removal of the $PC_{61}BM$ top-layer by diiodomethane (DIM) (Figure 2d). The P3HT(CB) and P3HT(CB-CN) bottom-layer after removal of the $PC_{61}BM$ top-layer, which will be denoted as P3HT(CB)/[$PC_{61}BM$] and P3HT(CB-CN)/[$PC_{61}BM$]. Since the absorption peak of $PC_{61}BM$ disappears at 300–400 nm after removal of the $PC_{61}BM$ top-layer, it is thought that the $PC_{61}BM$ was mostly removed by DIM. Slight decreases in the absorption intensity (around 4%∼7%) were observed for both P3HT(CB) and P3HT(CB-CN) films after removal of $PC_{61}BM$ from the corresponding bilayers. However, the overall shape of the P3HT absorption is the same after removal of the $PC_{61}BM$ layer. This, again, indicates that both P3HT films are suitable for the construction of a bilayer with the sequential solution process.

To investigate the heterojunction morphology formed at the P3HT/$PC_{61}BM$ interface, the $PC_{61}BM$ top-layer was selectively removed from the bilayer films using DIM. Figure 1c,d show the surface morphology and height profile of the P3HT(CB) and P3HT(CB-CN) bottom-layer after removal of the $PC_{61}BM$ top-layer. There is no apparent change in the surface morphology of the P3HT(CB)/[$PC_{61}BM$] and P3HT(CB-CN)/[$PC_{61}BM$] films compared to that of the P3HT(CB) and P3HT(CB-CN) films, respectively. This implies that the $PC_{61}BM$ layer coating process did not significantly influence the pre-formed morphology of the P3HT(CB-CN) and P3HT(CB) layers and that the surface morphology of the P3HT film is critical in the formation of the nano-scale heterojunction of the P3HT/$PC_{61}BM$ bilayer with a large surface area.

Both the P3HT(CB) and P3HT(CB-CN) films showed significant photoluminescence (PL) quenching (Figure 3) after deposition of the $PC_{61}BM$ top-layer. The PL intensity of the P3HT was quenched to 99.9% after construction of the P3HT(CB-CN)/$PC_{61}BM$ bilayer film, whereas the PL intensity was quenched to 97% after construction of the P3HT(CB)/$PC_{61}BM$ bilayer. Although detailed investigations on the possible reasons for the PL quenching is necessary, it seems that excitons are effectively dissociated in both bilayer films.

Although, there is little change in the surface morphology after deposition of the $PC_{61}BM$ layer by the SqSD process, a highly mobile $PC_{61}BM$ could inter-diffuse into the amorphous or less crystalline P3HT domain during the solution deposition process. To investigate the effect of the roughened P3HT on the bilayer OPV irrespective of the inter-mixing of P3HT and fullerene, P3HT/C_{70} bilayers were fabricated by thermal evaporation of C_{70} onto the P3HT bottom-layer. Sakai *et al.* fabricated a sequence of pentacene ultra-thin films of 1 nm thickness and C_{60} ultra-thin films of 1 nm thickness with a total active layer thickness of 50 nm by an alternating thermal evaporation method. After conducting cross sectional TEM experiments on the film, they found the alternating layer showed multilayers instead of forming inter-mixed layer [24]. Based on their result, the evaporated C_{70} was expected to form a bilayer with P3HT with little inter-diffusion and the heterojunction area of P3HT/C_{70} will be almost the same with surface area of P3HT bottom layer. The fabricated bilayers of P3HT(CB)/C_{70} and P3HT(CB-CN)/C_{70}

were utilized for fabrication of the solar cell with the structure ITO/PEDOT:PSS/Bilayer/BCP/Ag. Figure 4a compares the current density-voltage characteristics of the bilayer solar cells, and their solar cell parameters are listed in Table 2. The bilayer solar cell utilizing P3HT(CB-CN)/C_{70} exhibited an open-circuit voltage (V_{OC}) of 0.22 V, a short-circuit current density (J_{SC}) of 2.87 mA/cm^2, a fill factor (*FF*) of 0.50, and a power conversion efficiency (PCE) of 0.32%. The PCE of P3HT(CB-CN)/C_{70} is 14% higher than that of P3HT(CB)/C_{70}, which exhibited a V_{OC} of 0.22 V, a J_{SC} of 2.59 mA/cm^2, an *FF* of 0.48, and a PCE of 0.28%. The low V_{OC} of the bilayer is due to the small LUMO energy level of C_{70} (4.2 eV) compared to that of $PC_{61}BM$ (3.91 eV) [18,19]. It is worthwhile to note that the J_{SC} of P3HT(CB-CN)/C_{70} is 10.8% higher than that of P3HT(CB)/C_{70}.

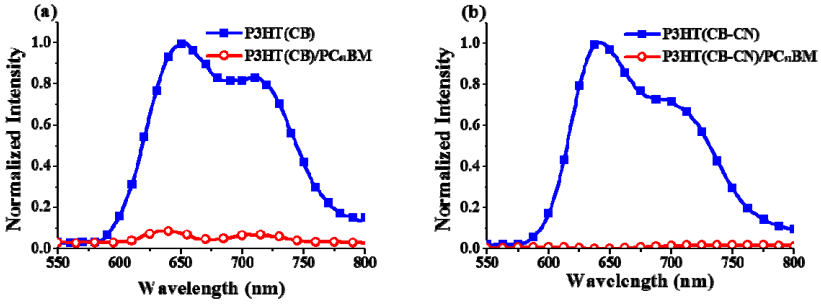

Figure 3. PL spectra of the P3HT and P3HT/$PC_{61}BM$ bilayer, (**a**) as-prepared P3HT(CB) bottom-layer (square) and P3HT(CB)/$PC_{61}BM$ bilayer (circle); and (**b**) as-prepared P3HT(CB-CN) bottom-layer (square) and P3HT(CB-CN)/$PC_{61}BM$ bilayer (circle).

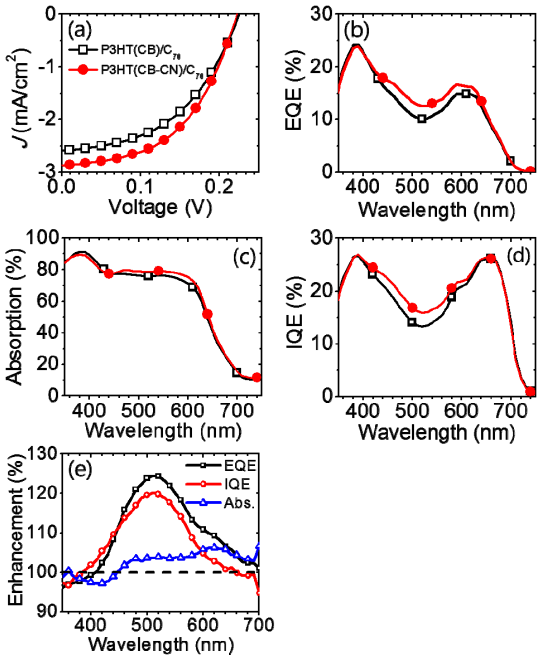

Figure 4. (**a**) Current density (*J*) *vs.* voltage (*V*) curves; (**b**) EQE spectra; (**c**) absorption intensity; and (**d**) IQE spectra of P3HT(CB)/C_{70} bilayer (black open square) and P3HT(CB-CN)/C_{70} bilayer OPVs (red solid circle); and (**e**) relative enhancement of absorption intensity and IQE values of P3HT(CB-CN)/C_{70} bilayer OPVs compared to those of P3HT(CN)/C_{70}.

Table 2. Solar cell parameters of bilayer OPVs based on the P3HT/C_{70} bilayer OPVs.

Active Layer	V_{OC} (V)	J_{SC} (mA/cm^2)	*FF*	PCE (%)
P3HT(CB)/C_{70}	0.22	2.59	0.48	0.28
P3HT(CB-CN)/C_{70}	0.22	2.87	0.50	0.32

It was found that both the improved absorption (Figure 4c) and the internal quantum efficiency (IQE) (Figure 4d) contribute to enhancing the EQE values of the P3HT(CB-CN)/C_{70} solar cell at a wavelength of 400–600 nm (Figure 4b). The absorption by the device was extracted from the measured wavelength-dependent reflectance data. The internal quantum efficiency (IQE) as a function of wavelength λ was determined as follows: IQE (λ) = EQE (λ)/[1 − R_{device}(λ)]. Since the same ITO-coated glass and Al electrode were used, it is thought that the difference between R_{device} values of P3HT(CB)/C_{70} and P3HT(CB-CN)/C_{70} is mainly ascribed to the difference between absorption intensities of the active layers. The absorption intensity of P3HT(CB-CN)/C_{70} was higher than that of P3HT(CB)/C_{70} at wavelengths between 500 and 650 nm, which corresponds to the absorption from the ordered P3HT chains. Since the absorption cross-sections can also be influenced by the molecular environment and packing, a P3HT(CB-CN) film that has more ordered domains than P3HT(CB) shows higher absorption intensity especially at 500–650 nm [23,25–27].

The improved IQE of P3HT(CB-CN)/C_{70} is thought to be attributed to the roughened P3HT(CB-CN) surface, which will enhance the exciton dissociation and charge collection efficiency of the P3HT(CB-CN)/C_{70}. To decide which factor, the absorption or the IQE improvement, contributes more to the higher EQE of the P3HT(CB-CN)/C_{70} solar cell, the relative enhancement of the absorption and IQE was obtained by dividing the corresponding value of P3HT(CB)/C_{70} by that of P3HT(CB-CN)/C_{70} (Figure 4e). Based on this analysis, the enhancement in EQE of the P3HT(CB-CN)/PC_{61}BM solar cell is mainly attributed to the improvement in the IQE of the P3HT(CB-CN)/PC_{61}BM rather than improvement in the absorption intensity of the P3HT(CB-CN) film. This reflects that the enhanced charge collection efficiency attributed by roughened P3HT surface mainly contributes to the improved solar cell performance rather than attributed by enhanced absorption of P3HT.

The SqSD-processed P3HT(CB)/PC_{61}BM and the P3HT(CB-CN)/PC_{61}BM bilayers were utilized to fabricate a bilayer OPV with the structure ITO/PEDOT:PSS/Bilayer/LiF/Al. Figure 5a compares current density-voltage characteristics of the bilayer OPV cells, and their parameters are listed in Table 3. We have tested four devices on each condition. The average efficiency and standard deviation of the OPVs were also included in the Table 3. The best bilayer OPV cell utilizing P3HT(CB-CN)/PC_{61}BM exhibited a V_{OC} of 0.63 V, a J_{SC} of 7.89 mA/cm^2, an *FF* of 0.66, and a PCE of 3.25%. The PCE of the P3HT(CB-CN)/PC_{61}BM is 25% higher than that of P3HT(CB)/PC_{61}BM, which exhibited a V_{OC} of 0.60 V, a J_{SC} of 7.43 mA/cm^2, an *FF* of 0.58, and a PCE of 2.59%. The bilayer prepared by the solution process is consistent with the results obtained by the vacuum deposition process. As shown in Figure 5b, the external quantum efficiency (EQE) spectra of the P3HT(CB)/PC_{61}BM and P3HT(CB-CN)/PC_{61}BM OPVs supports the J_{SC} result. The EQE value of P3HT(CB-CN)/PC_{61}BM was higher than that of P3HT(CB)/PC_{61}BM at wavelengths between 500 and 650 nm, which is coincident with the EQE spectra of P3HT(CB-CN)/C_{70}.Figure 5c shows PCE changes as a function of 1-CN concentration in the P3HT

solution. The PCE trend is exactly matching with the trend of surface roughness of P3HT (Figure 1e). This clearly shows the heterojunction area influences on the performance of SqSD processed bilayer OPVs. And the heterojunction area could be influenced by the surface roughness of P3HT bottom layer.

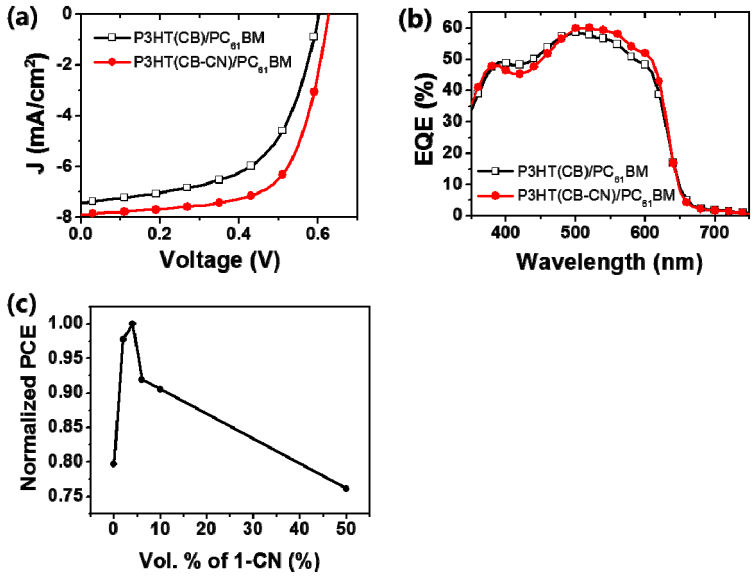

Figure 5. (**a**) Current density (*J*) *vs.* voltage (*V*) curves of bilayer OPVs based on the P3HT/$PC_{61}BM$ bilayers with a different P3HT bottom-layer and (**b**) their EQE spectra. (**c**) PCE of OPVs as a function of 1-CN concentration in P3HT solution.

Table 3. Solar cell parameters of P3HT/$PC_{61}BM$ bilayer OPVs.

Active Layer	V_{OC} (V)	J_{SC} (mA/cm^2)	*FF*	PCE (Avg.) (%)	PCE (Max.) (%)
P3HT(CB)/$PC_{61}BM$	0.60	7.43	0.58	2.32 $\pm$ 0.33	2.59
P3HT(CB-CN)/$PC_{61}BM$	0.63	7.89	0.66	3.22 $\pm$ 0.025	3.25

4. Conclusions

In conclusion, a method to control the nano-scale surface morphology of the conjugated polymer was developed by utilizing a polymer chain OA. In this study 1-CN was used as the OA for the P3HT. The addition of 1-CN to the P3HT solution, P3HT(CB-CN), improved the chain ordering of the P3HT during the solution deposition process, and the surface of the P3HT(CB-CN) film was roughened due to the ordered domains of P3HT. Adding 4 vol % of 1-CN to the host solvent was optimal to improve the surface roughness of the P3HT film. The roughened surface of P3HT(CB-CN) enhanced the performance of the P3HT(CB-CN)/$PC_{61}BM$ bilayer OPV without a thermal annealing process, especially the J_{SC} and *FF* values. Based on the AFM, PL, EQE analyses of the P3HT(CB-CN)/$PC_{61}BM$ bilayer, the roughened surface of the P3HT(CB-CN) increases the heterojunction area at the P3HT(CB-CN)/$PC_{61}BM$ interface and improves both the charge collection efficiency of the P3HT(CB-CN)/$PC_{61}BM$ bilayer OPV and the absorption efficiency due to enhanced ordering of the P3HT(CB-CN). We believe this method affords a novel process to improve the solar cell performance of bilayer OPVs without a thermal annealing process. Although the improvement of efficiency by roughened P3HT surface seems trivial, it would become

significant for the highly-efficient polymers. We believe our SqSD process utilizing OA establishes an alternative to the blend solution deposition (BSD) process for the fabrication of efficient OPVs and also allows for the reassessment of polymers which have shown insufficient performance in BSD process. Recently, we indeed observed that several polymers fabricated with our SqSD process exhibited better performance than those fabricated with the BSD process, which will be published elsewhere in the near future.

Acknowledgments

This research was supported by the Global Frontier R & D Program on Center for Multi-scale Energy System funded by the National Research Foundation under the Ministry of Science, ICT & Future Planning, Korea (No. 2011-0031567) and supported by the New & Renewable Energy Core Technology Program of the Korea Institute of Energy Technology Evaluation and Planning (KETEP), granted financial resource from the Ministry of Trade, Industry & Energy, Republic of Korea. (No. 20133030011330 and 20123010010140). We thank Kris Rathwell for the valuable discussions.

Author Contributions

Kyungkon Kim designed the experiments and wrote the manuscript. Yoonhee Jang, Ji-Won Seo and Jeesoo Seok carried out the experiments, film and device fabrication and analysis. Jung-Yong Lee carried out the IQE calculation on the OPV devices. All authors discussed the data and commented on the manuscript.

Conflicts of Interest

The authors declare no conflict of interest.

References

1. Yu, G.; Gao, J.; Hummelen, J.C.; Wudl, F.; Heeger, A.J. Polymer photovoltaic cells: Enhanced efficiencies via a network of internal donor–acceptor heterojunctions. *Science* **1995**, *270*, 1789–1790. [CrossRef]
2. Kim, K.; Liu, J.; Namboothiry, M.A.; Carroll, D.L. Roles of donor and acceptor nanodomainsin 6% efficient thermally annealed polymer photovoltaics. *Appl. Phys. Lett.* **2007**, *90*, 163511. [CrossRef]
3. Lee, J.K.; Ma, W.L.; Brabec, C.J.; Yuen, J.; Moon, J.S.; Kim, J.Y.; Lee, K.; Bazan, G.C.; Heeger, A.J. Processing additives for improved efficiency from bulk heterojunction solar cells. *J. Am. Chem. Soc.* **2008**, *130*, 3619–3623. [CrossRef] [PubMed]
4. Ayzner, A.L.; Tassone, C.J.; Tolbert, S.H.; Schwartz, B.J. Reappraising the need for bulk heterojunctions in polymer—Fullerene photovoltaics: The role of carrier transport in all-solution-processed P3HT/PCBM bilayer solar cells. *J. Phys. Chem.* **2009**, *113*, 20050–20060. [CrossRef]

5. Lee, K.H.; Schwenn, P.E.; Smith, A.R.; Cavaye, H.; Shaw, P.E.; James, M.; Krueger, K.B.; Gentle, I.R.; Meredith, P.; Burn, P.L. Morphology of all-solution-processed "bilayer" organic solar cells. *Adv. Mater.* **2011**, *23*, 766–770. [CrossRef] [PubMed]
6. Osaka, I.; McCullough, D. Advances in molecular design and synthesis of regioregular polythiophenes. *Acc. Chem. Res.* **2008**, *41*, 1202–1214. [CrossRef] [PubMed]
7. Marrocchi, A.; Lanari, D.; Facchetti, A.; Vaccaro, L. Poly(3-hexylthiophene): Synthetic methodologies and properties in bulk heterojunction solar cells. *Energy Environ. Sci.* **2012**, *5*, 8457–8474. [CrossRef]
8. Vohra, V.; Arrighetti, G.; Barba, L.; Higashimine, K.; Porzio, W.; Murata, H. Enhanced vertical concentration gradient in rubbed P3HT:PCBM graded bilayer solar cells. *J. Phys. Chem. Lett.* **2012**, *3*, 1820–1823. [CrossRef]
9. Ayzner, A.L.; Doan, S.C.; TremoletdeVillers, B.; Schwartz, B.J. Ultrafast studies of exciton migration andpolaronformation in sequentially solution-processed conjugated polymer/fullerene quasi-bilayer photovoltaics. *J. Phys. Chem. Lett.* **2012**, *3*, 2281–2287. [CrossRef]
10. Zhang, G.; Huber, R.C.; Ferreira, A.S.; Boyd, S.D.; Luscombe, C.K.; Tolbert, S.H.; Schwartz, B.J. Crystallinity effects in sequentially processed and blend-cast bulk-heterojunction polymer/fullerene photovoltaics. *J. Phys. Chem.* **2014**, *118*, 18424–18435. [CrossRef]
11. Lee, K.H.; Zhang, Y.; Burn, P.L.; Gentle, I.R.; James, M.; Nelson, A.; Meredith, P. Correlation of diffusion and performance in sequentially processed P3HT/PCBM heterojunction films by time-resolvedneutron reflectometry. *J. Mater. Chem.* **2013**, *1*, 2593–2598.
12. Hawks, S.A.; Aguirre, J.C.; Schelhas, L.T.; Thompson, R.J.; Huber, R.C.; Ferreira, A.S.; Zhang, G.; Herzing, A.A.; Tolbert, S.H.; Schwartz, B.J. Comparing matched polymer:Fullerene solar cells made by solution-sequential processing and traditional blend casting: Nanoscale structure and device performance. *J. Phys. Chem.* **2014**, *118*, 17413–17425. [CrossRef]
13. Clulow, A.J.; Tao, C.; Lee, K.H.; Velusamy, M.; McEwan, J.A.; Shaw, P.E.; Yamada, N.L.; James, M.; Burn, P.L.; Gentle, I.R.; *et al*. Time-resolved neutron reflectometry and photovoltaic device studies on sequentially deposited PCDTBT-Fullerene layers. *Langmuir* **2014**, *38*, 11474–11484. [CrossRef] [PubMed]
14. Nardes, A.M.; Ayzner, A.L.; Hammond, S.R.; Ferguson, A.J.; Schwartz, B.J.; Kopidakis, N. Photoinduced charge carrier generation and decay in sequentially deposited polymer/fullerene layers: Bulk heterojunction *vs*. planar interface. *J. Phys. Chem.* **2012**, *116*, 7293–7305. [CrossRef]
15. Gadisa, A.; Tumbleston, J.R.; Ko, D.-H.; Aryal, M.; Lopez, R.; Samulski, E.T. The role of solvent and morphology on miscibility of methanofullerene and poly(3-hexylthiophene). *Thin Solid Films* **2012**, *520*, 5466–5471. [CrossRef]
16. Ramanathan, M.; MichaelKilbey, S., II; Ji, Q.; Hill, J.P.; Ariga, K. Materials self-assembly and fabrication in confined spaces. *J. Mater. Chem.* **2012**, *22*, 10389–10405. [CrossRef]
17. Xiong, K.; Hou, L.; Wu, M.; Huo, Y.; Mo, W.; Yuan, Y.; Sun, S.; Xu, W.; Wang, E. From spin coating to doctor blading: A systematic study on the photovoltaic performance of anisoindigo-based polymer. *Sol. Energy Mater. Sol. Cells* **2015**, *132*, 252–259. [CrossRef]

18. Guo, S.; Herzig, E.M.; Naumann, A.; Tainter, G.; Perlich, J.; Müller-Buschbaum, P. Influence of solvent and solvent additive on the morphology of PTB7 films probed via X-ray scattering. *J. Phys. Chem.* **2013**, *118*, 344–350. [CrossRef] [PubMed]
19. Beaujuge, P.M.; Fréchet, J.M. Molecular design and ordering effects in π-functional materials for transistor and solar cell applications. *J. Am. Chem. Soc.* **2011**, *133*, 20009–20029. [CrossRef] [PubMed]
20. Hoven, C.V.; Dang, X.D.; Coffin, R.C.; Peet, J.; Nguyen, T.Q.; Bazan, G.C. Improved performance of polymer bulk heterojunction solar cells through the reduction of phase separation via solvent additives. *Adv. Mater.* **2010**, *22*, E63–E66. [CrossRef] [PubMed]
21. Wu, M.-C.; Lin, Y.-Y.; Chen, S.; Liao, H.-C.; Wu, Y.-J.; Chen, C.-W.; Chen, Y.-F.; Su, W.-F. Enhancing light absorption and carrier transport of P3HT by doping multi-wall carbon nanotubes. *Chem. Phys. Lett.* **2009**, *468*, 64–68. [CrossRef]
22. Vanlaeke, P.; Swinnen, A.; Haeldermans, I.; Vanhoyland, G.; Aernouts, T.; Cheyns, D.; Deibel, C.; D'Haen, J.; Heremans, P.; Poortmans, J. P3HT/PCBM bulk heterojunction solar cells: Relation between morphology and electro-optical characteristics. *Sol. Energy Mater. Sol. Cells* **2006**, *90*, 2150–2158. [CrossRef]
23. Salim, T.; Wong, L.H.; Bräuer, B.; Kukreja, R.; Foo, Y.L.; Bao, Z.; Lam, Y.M. Solvent additives and their effects on blend morphologies of bulk heterojunctions. *J. Mater. Chem.* **2011**, *21*, 242–250. [CrossRef]
24. Sakai, J.; Taima, T.; Yamanari, T.; Yoshida, Y.; Fujii, A.; Ozaki, M. Pentacene:Fullerene multilayer-heterojunction organic photovoltaic cells fabricated by alternating evaporation method. *Jpn. J. Appl. Phys.* **2010**, *49*, 032301. [CrossRef]
25. Heremans, P.; Cheyns, D.; Rand, B.P. Strategies for increasing the efficiency of heterojunction organic solar cells: Material selection and device architecture. *Acc. Chem. Res.* **2009**, *42*, 1740–1747. [CrossRef] [PubMed]
26. Slota, J.E.; He, X.; Huck, W.T. Controlling nanoscale morphology in polymer photovoltaic devices. *Nano Today* **2010**, *5*, 231–242. [CrossRef]
27. Erb, T.; Zhokhavets, U.; Gobsch, G.; Raleva, S.; Stühn, B.; Schilinsky, P.; Waldauf, C.; Brabec, C.J. Correlation between structural and optical properties of composite polymer/fullerene films for organic solar cells. *Adv. Funct. Mater.* **2005**, *15*, 1193–1196. [CrossRef]